Investigating self-organised criticality of a simulated rice pile using the Oslo model

Ben R. Amroota

CID: 01508466

19th February 2021

***Abstract*— This project details an investigation into self-organised criticality for different system sizes $L = \{4, 8, 16, 32, 64, 128, 256\}$ using the Oslo model. Self-organised criticality is a characteristic possessed of some dynamic systems with an attractor state, and results in non-trivial behaviour for complex systems. A computer program is written in Python to implement the model, investigate possible corrections to scaling and deduce the mathematical form of the scaling functions. Various properties of the system are explored including the heights of the system, cross-over times, standard deviations, avalanche size probabilities, and the avalanche sizes. This enables a finite-size scaling ansatz to be adopted to model the associated corrections to scaling. The critical exponents of the system are estimated using moment analysis with the finite-size scaling ansatz to be $D = 2.25 \pm 0.05$ and $\tau_s = 1.56 \pm 0.05$. Word Count - 2478**

I. INTRODUCTION

THE Oslo model is a generalisation of the 1-dimensional Bak-Tang-Weisenfield model and provides a clear framework for complex systems displaying self-organised criticality [1] [2][3]. The model uses a pile of rice grains to simulate the addition of energy to a system and the dissipation of the energy in the form of events, in this case avalanches.

A complex system is described as self-organised if the system reaches a steady state with no fine-tuning of external parameters, and critical if the avalanche sizes are scale-free; there is no typical size of an avalanche. Thus, the response of the system to a change in the system is independent of the change.

II. IMPLEMENTATION OF THE OSLO MODEL

The Oslo model is a 1-dimensional model of a ricepile demonstrating self-organised criticality [2]. Such a sandpile is modelled as a 1D lattice of L sites, $i = 1, 2, \dots, L$, each assigned an associated threshold slope $z_i^{th} \in \{1, 2\}$. The threshold slopes are chosen using a random number generator such that

$$P(z_i^{th} = 1) = p\,, \qquad P(z_i^{th} = 2) = 1 - p\,. \tag{1}$$

The system is initialised with a lattice size L and a probability p as defined above. The system is driven by adding a single grain to the leftmost site, $i = 1$, and relaxes when the slope at site i z_i exceeds the threshold slope. Upon the grain toppling to site $i + 1$, a new threshold slope z_i^{th} is randomly assigned using equation (1). The threshold slope z_i^{th} is only reassigned if the site i relaxes. The avalanche size is defined as the total number of relaxations following the addition of a single grain. The system begins in the set of transient configurations which appear at most once, but eventually reaches a set of recurrent configurations which are revisited indefinitely if the system is driven indefinitely; the latter is a statistically stationary state.

A. Implementation Testing

For the original Oslo model ($p = 0.5$) the average avalanche size $\langle s \rangle$ in the indefinitely driven steady state is given by

$$\langle s \rangle = L\,, \tag{2}$$

since in the steady state the average number of grains added to the system equals the average number of grains leaving the system. The simulation is driven 1.5 million times and the resulting time-averaged avalanche sizes divided by the system size are plotted in Fig. 1. This shows that the average avalanche size divided by system size is 1.00 within appreciable bounds of error, hence the implementation is correctly executed.

To further test the implementation, the height of the pile $h(t;L)$ is defined to be the height of site i =1 at time t. The time-averaged height of the pile is measured for $L = 16$ and $L = 32$ to be 26.53 ± 1.14 and 53.89 ± 1.34 respectively, in agreement with theoretical values [4].

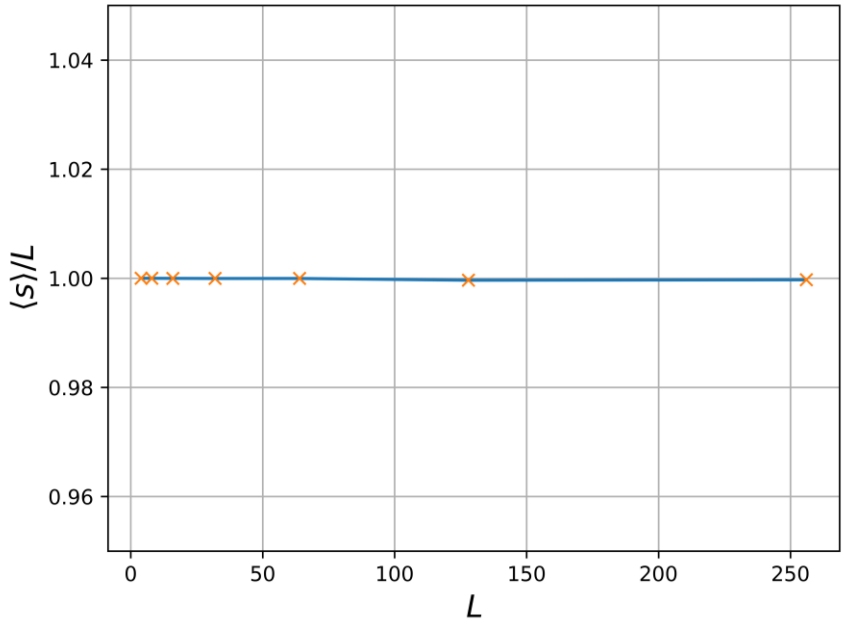

Fig. 1. The relationship between the average avalanche size divided by system size and system size. The average avalanche size is found to be equal to the system size within appreciable bounds of error, and so displays a horizontal straight-line graph with a y-intercept of 1.00, thus indicating the Oslo model is correctly implemented.

In the limit $p = 1$ the Oslo model reduces to the 1-dimensional Bak-Tang-Wiesenfield model, thus in the steady state

$$h(t;L) = s = L\,. \tag{3}$$

The simulation is driven 50,000 times and the measured values in the steady state for the height, avalanche size and number of grains are shown in Table. 1.

L	$h(t;L)$	s	N
16	16	16	136
32	32	32	528
128	128	128	8256

Table. 1. The observed heights, avalanche sizes and number of grains in the pile N in the steady state for the Oslo model with $p = 1$. In the steady state, only those values listed above are measured, hence there is no error associated with these quantities. The system has reached the single configuration in the steady state and equation (3) is observed.

The results are as expected: the BTW model only has one recurrent configuration, indicated by the single value of N measured in the attractor state, and $h(t;L) = s = L$. In the limit that $p = 0$, the Oslo model reduces to the BTW model, but $h = 2L$. Running the simulation for $p = 0$ returns the values shown in Table. 2, and verifies that the implementation is correct. Testing the edge cases $p = 0.05$ and $p = 0.95$ returns expected results: there are more than one

recurrent configurations with slightly lower and higher average heights respectively than for the boundary cases. The generic, boundary and edge cases have therefore shown to be correctly implemented.

L	$h(t;L)$	s	N
16	32	16	272
32	64	32	1056
128	256	128	16512

Table. 2. The measured heights, avalanche sizes and number of grains in the pile N in the steady state for the Oslo model with $p = 0$. As in Table. 1, in the steady state, only a single value for each of the quantities is observed, as there is only one recurrent configuration. Therefore, there is no error associated with these quantities.

III. THE HEIGHT OF THE PILE

A. Transient and Recurrent Configurations

During the set of transient configurations, the system acts as if infinite, and the height of the pile increases with grain additions. The system eventually reaches the steady state, and so the time-averaged height of the pile approaches a constant value, as in Fig. 2. There are multiple recurrent configurations which are revisited indefinitely for an indefinitely driven system, seen in Fig. 3 for $L = 4$. Each configuration has a different height, leading to some associated statistical error in the average height of the pile. The progression of the system to a set of recurrent configurations is a symptom of self-organisation.

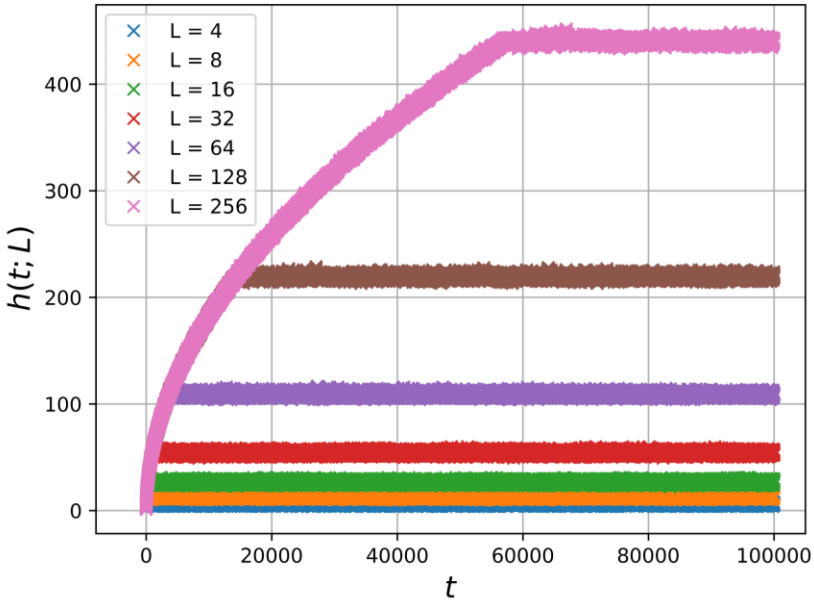

Fig. 2. The height of the pile as a function of time elapsed. The height increases following a power law in time whilst in the transient set of configurations. Once the attractor of the dynamics is reached the average height reaches a constant value, and the system occupies the set of recurrent configurations.

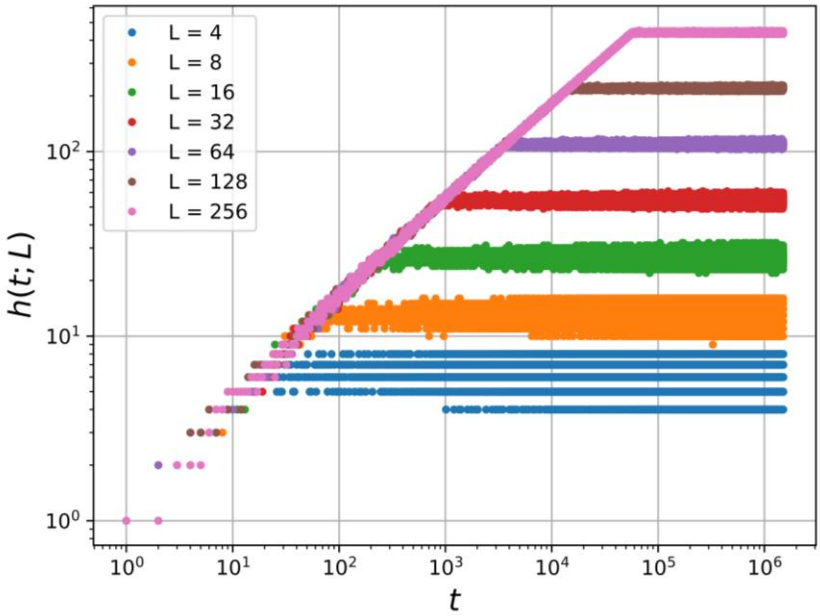

Fig. 3. The log-log relationship between the height of the pile and the number of grains added. Smaller ticks are used to highlight the multiple recurrent configurations present in the attractor state, as can be clearly observed for $L = 4$.

B. The cross-over time

The cross-over time t_c is defined as the number of grains in the system before the addition of a grain results in the first grain leaving the system. This is calculated by noting when the boundary condition for the site $i = L$ is activated for the first time and measuring the number of grains in the system at that point. The Oslo model is implemented 10 times for 100,000 grain additions, and the average cross-over times $\langle t_c \rangle$ are shown in Fig. 4. Hence, in the limit $L \gg 1$ the average cross-over time obeys a power law

$$\langle t_c \rangle = aL^b \, . \tag{4}$$

The parameters a and b are calculated from the fit, seen in red, to be 0.83 ± 0.01 and 2.01 ± 0.01 respectively. Hence, the average cross-over time scales like L^2 for $L \gg 1$, $\langle t_c \rangle \propto L^2$.

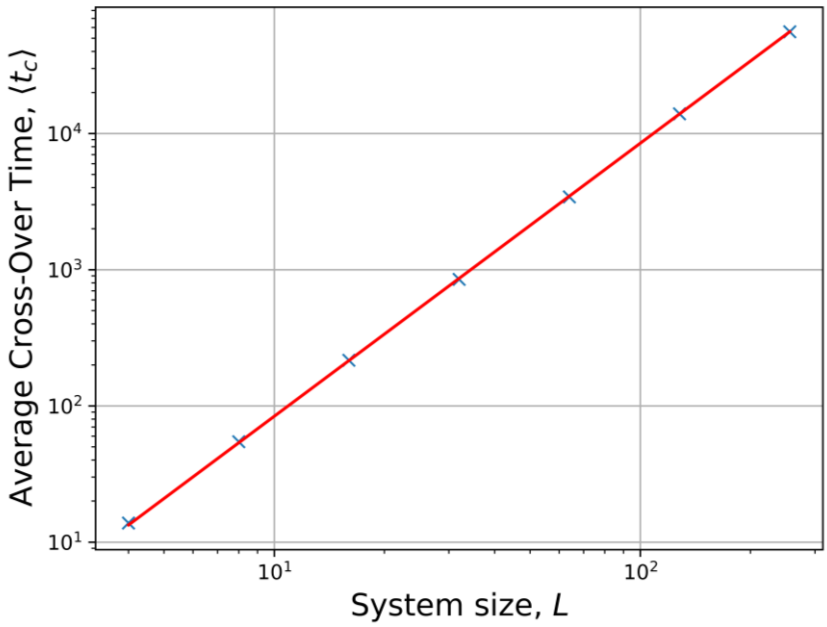

Fig. 4. The log-log relationship between the average cross-over time and the system size. The linear relationship observed in the log-log plot indicates that the average cross-over time is related to system size by a power law. The power law fitted is plotted in red.

C. Scaling behaviour for $L \gg 1$

When the system reaches the steady state the average number of grains in the system is constant. Thus, for the slowly singly driven case, it is anticipated that a single grain entering the system induces an avalanche of average size L causing a single grain to leave the system. The average slope of the system $\langle z(t)\rangle_t$ will vary in time around some constant value. Mathematically,

$$h(t;L) = \sum_{i=1}^{L} z_i(t) = L\frac{1}{L}\sum_{i=1}^{L} z_i(t) = L\langle z(t)\rangle_i \,, \tag{5}$$

therefore

$$\langle h(t;L)\rangle_t = L\langle z(t)\rangle_{i,t} \,. \tag{6}$$

Assuming that in the steady state $\langle z\rangle$ is independent of the system size for $L \gg 1$,

$$\langle h(t;L)\rangle_t = L\langle z(t)\rangle_t \propto L \,. \tag{7}$$

The cross-over time is defined to be the total number of grains in the system before the first grain leaves the system. The slope at the cross-over time averaged over M different realisations varies around some constant value. Hence, in the limit $L \gg 1$ corrections to scaling can be neglected and the cross-over time can be approximated as the area of the ricepile,

$$\langle t_c\rangle_M = \frac{1}{2}\langle h(t;L)\rangle_M L \,. \tag{8}$$

This yields

$$\langle t_c\rangle_M = \frac{1}{2}L\langle z(t_c)\rangle_M L \propto L^2 \,. \tag{9}$$

The time-averaged height in the steady state should thus scale linearly with system size and the average of the cross-over time should scale quadratically with system size.

D. Data Collapse

The processed height $\tilde{h}(t;L)$ is the average of the heights at time t over M realisations. A data collapse is performed by considering the theoretical relationships

$$\begin{aligned} \langle t_c\rangle_M &\propto L^2 \,, \\ \langle h(t;L)\rangle_t &\propto L \,. \end{aligned} \tag{10}$$

The data collapse is facilitated by dividing the left-hand side of equation (10) by the right-hand side, accounting for their respective dependencies on system size. In the steady state the left-hand side of equation (11) is thus a function of one variable whereas the right-hand side is a function of two variables. This introduces the scaling function $\mathcal{F}(t/L^2)$,

$$\frac{\tilde{h}(t;L)}{L} = \mathcal{F}\left(\frac{t}{L^2}\right). \tag{11}$$

The plot of $\tilde{h}(t;L)/L$ against t/L^2 collapses the data for different system sizes onto the single scaling function $\mathcal{F}(t/L^2)$, as seen in Fig. 5. The collapsed data does not align fully for small systems, this is attributed to corrections to scaling since equation (11) assumes $L \gg 1$.

In the limit that $t/L^2 \ll 1$, the system is still in the transient configuration and hence acts as if infinite: The grains have not yet reached the edge of the system, there is no information about the size of the system, and so $\tilde{h}(t;L)$ is L-independent. Thus, the scaling function satisfies

$$\mathcal{F}(t/L^2) \propto 1/L \,, \tag{12}$$

which can be written as

$$\mathcal{F}(t/L^2) \propto \sqrt{t/L^2} \propto \sqrt{t}/L \,. \tag{13}$$

In the limit that $t/L^2 \gg 1$, the system has reached the set of recurrent configurations and the time averaged height of the pile fluctuates around some constant value. The scaling function hence approaches a constant value, as can be seen in Fig. 5, and the processed height of the pile becomes

$$\tilde{h}(t;L) = constant \cdot L \,. \tag{14}$$

The dependency of the scaling function $\mathcal{F}(t/L^2)$ on t/L^2 is therefore such that, in the limit of $L \gg 1$,

$$\begin{aligned} \mathcal{F}(x \ll 1) &\propto \sqrt{x} \,, \\ \mathcal{F}(x \gg 1) &= constant = \langle z \rangle. \end{aligned} \tag{15}$$

The processed height of the pile in the transient state $t/L^2 \ll 1$, thus obeys

$$\tilde{h}(t;L) \propto L\frac{\sqrt{t}}{L} \propto \sqrt{t} \,. \tag{16}$$

Hence, it is predicted that in the transient $\tilde{h}(t;L) \propto \sqrt{t}$.

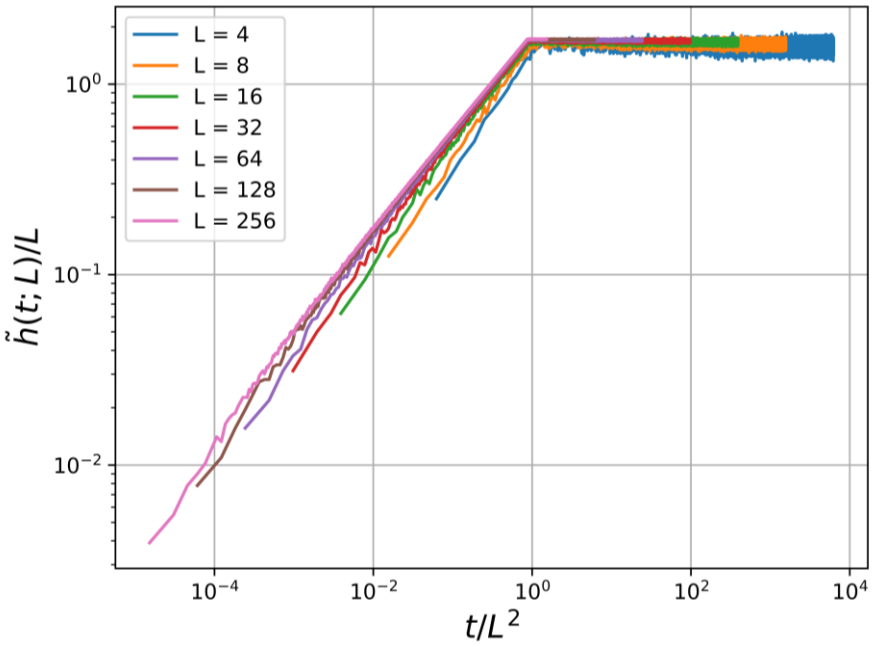

Fig. 5. The data collapse for the processed height of the system as a function of time for a set of system sizes L. The data collapses onto a single scaling function $\mathcal{F}(t/L^2)$ which obeys a power law in the transient and reduces to a constant in the steady state. The data does not fully align onto the same function for small system sizes, this is attributed to corrections to scaling as the data collapse is only valid for $L \gg 1$.

E. Corrections to scaling for the time-averaged height

Considering only first order corrections to scaling, the time-averaged height of the system after reaching steady state is

$$\langle h(t;L) \rangle_t = a_0 L(1 - a_1 L^{-\omega_1}) \,. \tag{17}$$

The time-averaged heights in the attractor are plotted against the system size in Fig. 6. The form of equation (17) is adopted as a fitting function, and a method of minimising the least-squares is used to return the fitting parameters a_0, a_1 and ω_1. The average slope in an infinite sized system satisfies

$$\langle z \rangle = \lim_{L \to \infty} \frac{\langle h \rangle}{L}, \tag{18}$$

therefore, it is anticipated that $\langle z \rangle = a_0$ for $L \to \infty$. As only first order corrections are being considered, the fit in Fig. 6 is only applied to the last four system sizes $L = \{32, 64, 128, 256\}$. The calculated fit parameters are estimated from the fitted function to be $a_0 = 1.73 \pm 0.01$, $a_1 = 0.27 \pm 0.05$ and $\omega_1 = 0.64 \pm 0.05$.

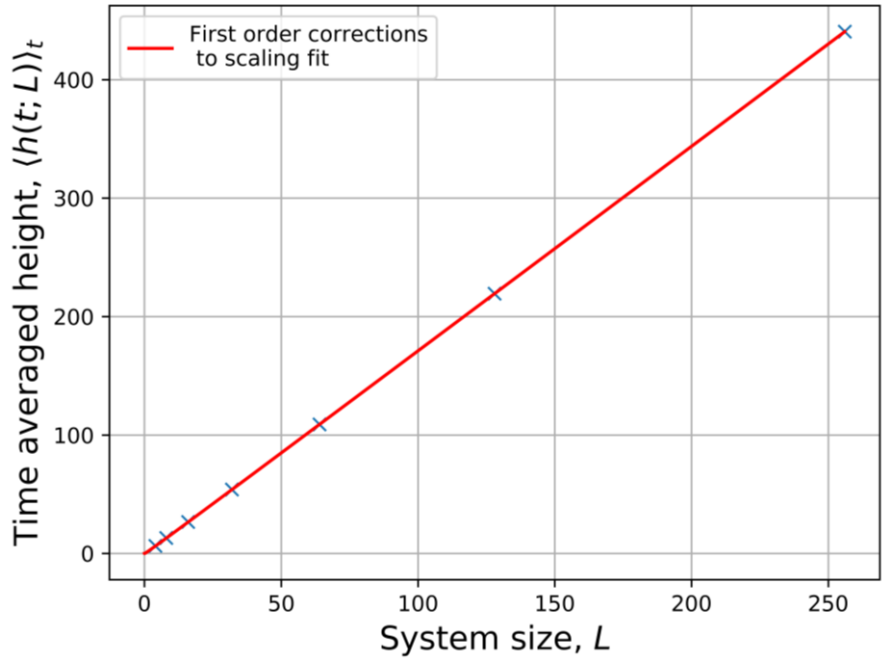

Fig. 6. The time averaged height of the system in the steady state as a function of system size. A fit describing the first order corrections to scaling is applied to only the last four system sizes $L = \{32, 64, 128, 256\}$ since the first order corrections to scaling alone do not allow the fit to be applied to lower system sizes.

F. The standard deviations of the height and slope

The standard deviation of the time-averaged heights in the steady state is calculated and plotted against the system size L in Fig. 7. The data follows a power law distribution in L

$$\sigma_h(L) = aL^b, \tag{19}$$

described by the fitted function in Fig. 7. The data deviates from the fit for small system sizes, because the function neglects corrections to scaling and is only valid for $L \gg 1$. The power law the fit is only applied to the four largest system sizes. By minimising the least-squares to estimate fit parameters, the standard deviation of the height is

$$\sigma_h(L) \propto L^{0.25 \pm 0.05}. \tag{20}$$

The system sizes are parameters of the system and do not have errors, hence in the steady state the standard deviation of the average slope of the system is

$$\sigma_{\langle z \rangle} = \frac{\sigma_h}{L}. \tag{22}$$

Therefore,

$$\sigma_{\langle z \rangle}(L) \propto \frac{L^{0.25 \pm 0.05}}{L} \propto L^{-0.75 \pm 0.05}, \tag{23}$$

and so, in the limit $L \to \infty$, $\sigma_{\langle z \rangle} = 0$ and $\langle z \rangle = a_0$.

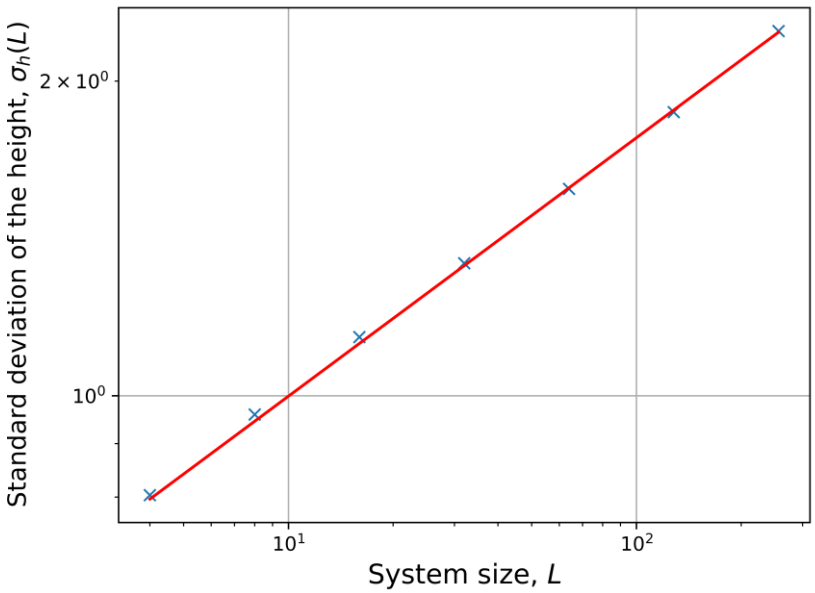

Fig. 7. The standard deviation of the heights as a function of system size. The relationship obeys a power law distribution, shown in red. The fit is only applied to the four largest system sizes since it neglects corrections to scaling and is therefore only valid for $L \gg 1$.

G. Scaling probability distributions

The height of the pile is given by the sum over the slopes $h = \sum_{i=1}^{L} z_i$. Assuming the individual slopes z_i are independent random variables, the central limit theorem can be invoked in the limit $L \gg 1$. The probability distribution is predicted to be Gaussian with standard deviation σ_h and mean $\langle h(t;L)\rangle$. If z_i are random, identically distributed, and independent the standard deviation of the slopes $\sigma_{\langle z\rangle}$ becomes

$$\sigma_{\langle z\rangle}(L) = \sqrt{\frac{1}{L-1}\sum_{i=1}^{L}(z-\bar{z})^2} \propto \frac{1}{\sqrt{L}}, \tag{24}$$

in the case of large L. It is therefore predicted that the height standard deviation scales as $\sigma_h \propto \sqrt{L}$. The height probabilities for different system sizes are plotted in Fig. 8.

The height probability distribution hence satisfies

$$P(h;L) = \frac{1}{\sigma_h\sqrt{2\pi}}\, e^{-\frac{1}{2}\left(\frac{h-\langle h\rangle}{\sigma_h}\right)^2}, \tag{25}$$

which can be rewritten as

$$P(h;L)\sigma_h = \frac{1}{\sqrt{2\pi}}\, e^{-\frac{1}{2}\left(\frac{h-\langle h\rangle}{\sigma_h}\right)^2}. \tag{26}$$

By defining $x = (h-\langle h\rangle)/\sigma_h$, the left-hand side of equation (25) can be written as a function of two variables, whereas the right-hand side can be written as a function of just one:

$$P(h;L)\sigma_h = \mathcal{F}(x)\,. \tag{27}$$

The data collapse is thus performed by plotting $P(h;L)\sigma_h$ against $(h-\langle h\rangle)/\sigma_h$, as in Fig. 9.

The data does not align with the gaussian, displaying a positive skew. The heights standard deviation theoretically scales like $\sigma_h \propto L^{0.5}$, but experimentally scales like $\sigma_h \propto L^{0.25\pm0.05}$. This discrepancy is attributed to invalid assumptions; z_i are not independent identically distributed variables because the relaxation conditions at the boundary sites $i = 1, L$ are different. This implies they are dependent, hence the poor data collapse in Fig. 9.

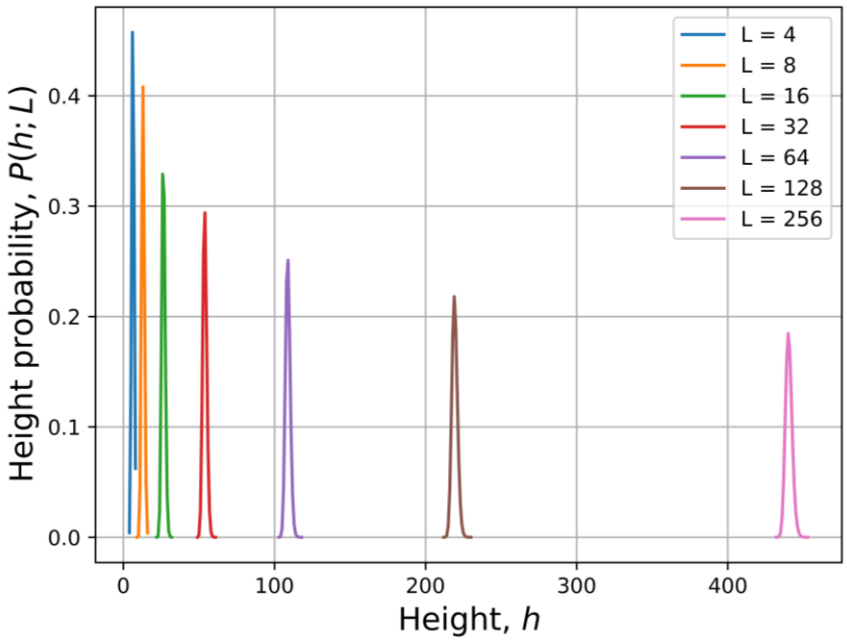

Fig. 8. The height probabilities as a function of height and system size. The standard deviation of the heights increases with system size and the height probability decreases with system size. This is because the number of recurrent configurations increases with system size, hence the number of configurations with a non-zero probability of being occupied also increases.

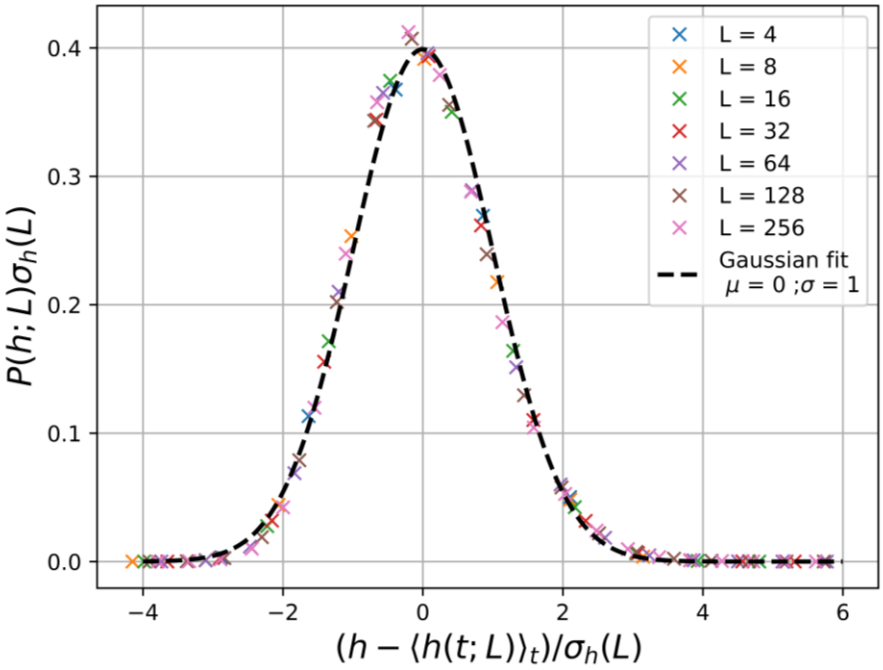

Fig. 9. The data collapse for the height probabilities for different system sizes. A gaussian centred on 0 and with width 1 is plotted to assess the validity of the use of the central limit theorem. The data does deviate from the theoretically predicted gaussian, displaying a slight positive skew. This is due to the invalid assumption that z_i are independent. A plot of the residuals of the fit would provide a quantitative measure of this deviation.

IV. THE AVALANCHE SIZE PROBABILITY

A. *Scaling avalanche size probabilities*

The avalanche size probability is plotted as a function of avalanche size in Fig. 10. There is a significant amount of noise in the plot tail, owing to poor statistics. Log-binning is applied to reduce this noise by splitting the x-axis into logarithmically increasing bins. The geometric means of the bins are calculated and used to calculate the probability that an avalanche of size s is located in the j^{th} bin $\tilde{P}_N(s;L)$. The probabilities $\tilde{P}_N(s;L)$ are plotted as a function of avalanche size in Fig. 11. Log-binning improves the clarity of data but loses information about exactly what size the avalanche is.

The avalanche size probabilities in Fig. 11 first obey a power-law decay in s, then peak before falling off asymptotically to a cut-off avalanche size s_c. The power law behaviour is typical of a system displaying criticality; avalanches are scale-free in the scaling region $1 \ll s \ll s_c$, and have no typical size except for a cut-off size which increases with system size. The cut-off avalanche size and hence the peak avalanche probability is imposed by the finite nature of the system. In a finite system the maximum avalanche size restricts the size of avalanches, leading to more avalanches bunching up in the region $s \to s_c$, hence the peak. The scaling region for $L = 4$ is absent due to the small system size.

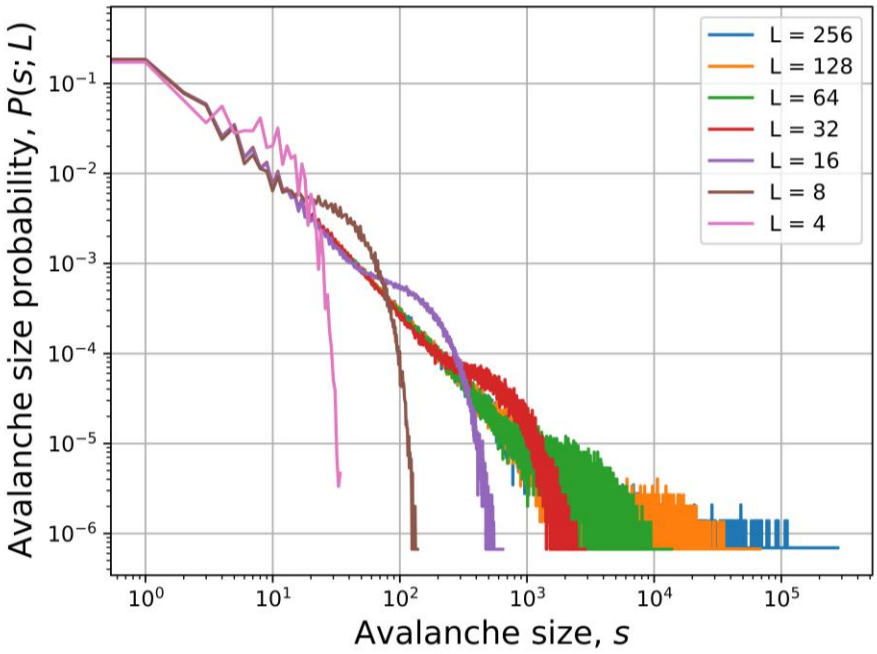

Fig. 10. The avalanche size probabilities as a function of avalanche size. The data is un-binned and hence displays large degrees of statistical noise in the tail region of the plot, attributed to poor statistics.

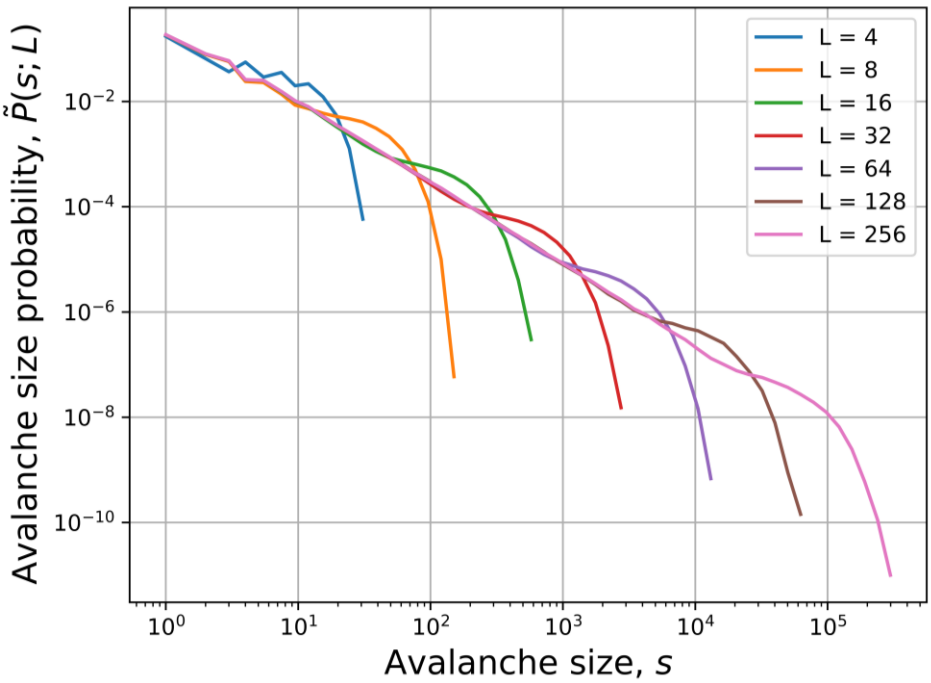

Fig. 11. The binned avalanche size probabilities as a function of avalanche size. The data is binned into logarithmically increasing bin widths and illustrates the scale-free behaviour of the system in the scaling region $1 \ll s \ll s_c$. The cut-off avalanche size is taken as the maximum avalanche size observed.

B. Finite-size scaling ansatz

A finite-size scaling ansatz is proposed of the form

$$\tilde{P}(s;L) = as^{-\tau_s}\mathcal{F}(s/s_c)\,, \qquad s_c(L) = bL^D, \tag{28}$$

for $L \gg 1$ and $s \gg 1$, where $\mathcal{F}(x \gg 1)$ decays rapidly. In this limit corrections to scaling can be neglected and therefore

$$P(s;L) \sim as^{-\tau_s}\,, \qquad s_c(L) \sim bL^D. \tag{29}$$

The critical exponents D and τ_s are estimated to be $D = 2.25 \pm 0.05$ and $\tau_s = 1.54 \pm 0.05$, using the fits in Fig. 12 and Fig. 13 respectively. These values are consistent with the expression associated with equation (2),

$$D(2-\tau_s) = 1.04 \pm 0.11\,. \tag{30}$$

The fits are only applied to the regions of the graphs where the above limits hold.

Equation (28) can be rearranged such that the left-hand side is a function of two variables whereas the right-hand side is a function of one,

$$\tilde{P}(s;L)s^{\tau_s} \propto \mathcal{F}(x)\,, \tag{31}$$

where $x = s/s_c \propto s/L^D$. In the limit $L \gg 1$ and $s \gg 1$, the data can be collapsed onto a single function if $P(s;L)s^{\tau_s}$ is plotted against s/L^D. This is done in Fig. 14 using the calculated critical exponents D and τ_s. The data collapses onto a single function for all but the smallest system size, hence the proposed finite-size scaling ansatz is found to be consistent with the log-binned avalanche size probabilities.

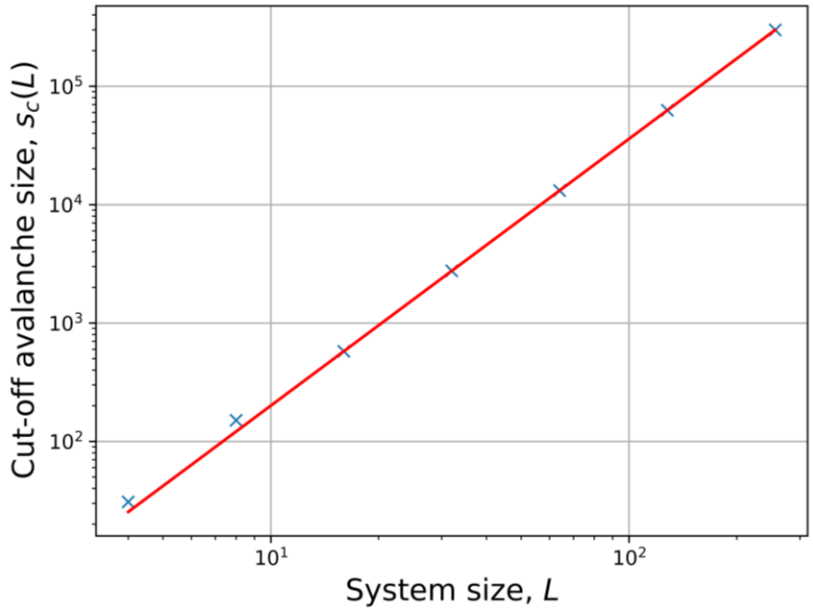

Fig. 12. The cut-off avalanche size as a function of system size. The relationship for $L \gg 1$ is described using a simple power law, seen in red, the exponent of which is the critical exponent D. The fit is only applied to the four largest system sizes since the fit neglects corrections to scaling, and hence is only valid $L \gg 1$. The maximum avalanche size from Fig. 11 is used as the cut-off avalanche size.

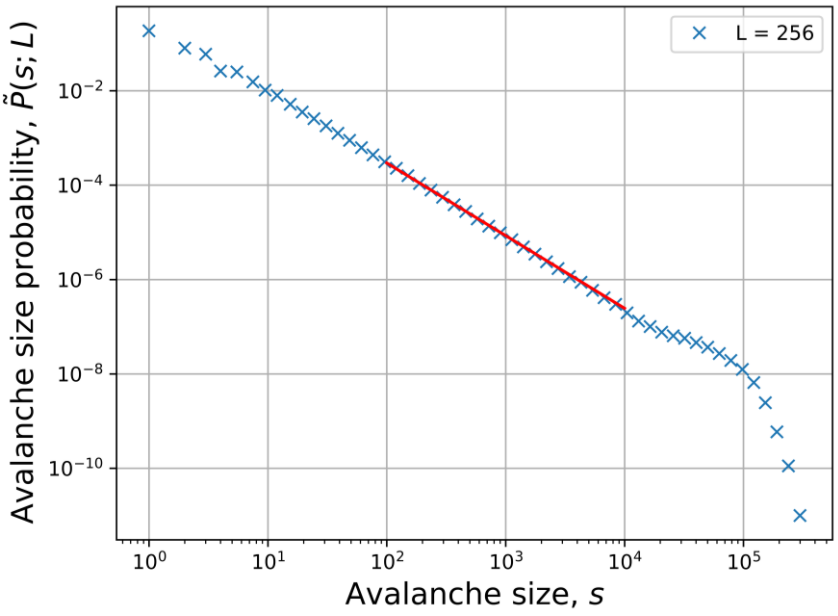

Fig. 13. The binned avalanche size probability as a function of avalanche size. A power-law fit is applied to the scaling region $1 \ll s \ll s_c$, to estimate the critical exponent τ_s. The $L = 256$ system size is used as it has the largest scaling region of the system sizes simulated.

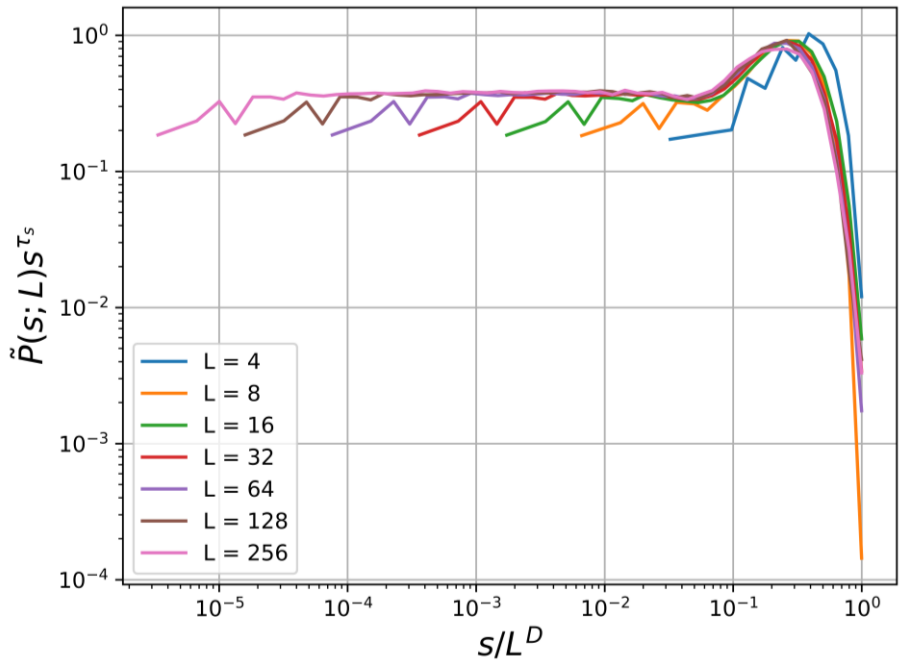

Fig. 14. The data collapse of the log-binned avalanche size probabilities. The critical exponents used are $D = 2.25 \pm 0.05$ and $\tau_s = 1.54 \pm 0.05$. The function seen is the scaling function for the Oslo model, and is a constant value for small arguments $s/L^D \ll 1$. For arguments $s/L^D \gg 1$, the scaling function rapidly decays. The smallest system size seen does not collapse onto the scaling function as it does not obey the required limit of $L \gg 1$.

C. *Moment analysis of avalanche sizes*

The k^{th} moment of the avalanche size is given by

$$\langle s^k \rangle = \lim_{T\to\infty} \frac{1}{T} \sum_{t=t_0+1}^{t_0+T} s_t^k = \sum_{s=1}^{\infty} s^k P(s;L)\,, \tag{32}$$

where s_t is the avalanche size measured at time t. Assuming the finite-size scaling ansatz proposed in equation (28),

$$\langle s^k \rangle = \sum_{s=1}^{\infty} s^k s^{-\tau_s} \mathcal{F}(s/L^D)\,. \tag{33}$$

If the predominant contribution to the k^{th} moment is from $s \gg 1$, the sum can be approximated as an integral, and using a change of variable $u = s/L^D$, this yields

$$\langle s^k \rangle = L^{D(1+k-\tau_s)} \int_{1/L^D}^{\infty} u^{k-\tau_s} \mathcal{F}(u) du\,. \tag{34}$$

The integral reduces to a finite number in the limit that $L \gg 1$ and provided $1 + k - \tau_s > 0$, therefore

$$\langle s^k \rangle \propto L^{D(1+k-\tau_s)}\,. \tag{35}$$

The measured k^{th} moments are plotted against system size in Fig. 15 showing a power law as anticipated. The FSS ansatz only holds in the limit $L \gg 1$: the data deviates from the fitted power laws for small system sizes. The exponent in equation (35) is estimated from the fitted functions in Fig. 15.

These are plotted against the moments in Fig. 16, for which the straight line has gradient D, calculated to be 2.25 ± 0.05, and intercepts the k-axis at $\tau_s - 1$, giving $\tau_s = 1.56 \pm 0.05$. These values are checked through use of equation (2), which in conjunction with equation (32), yields

$$D(2 - \tau_s) = 0.99 \pm 0.11 \,. \tag{36}$$

Therefore, the determined critical exponents satisfy the required relation within the bounds of error and prove that the system displays self-organised criticality.

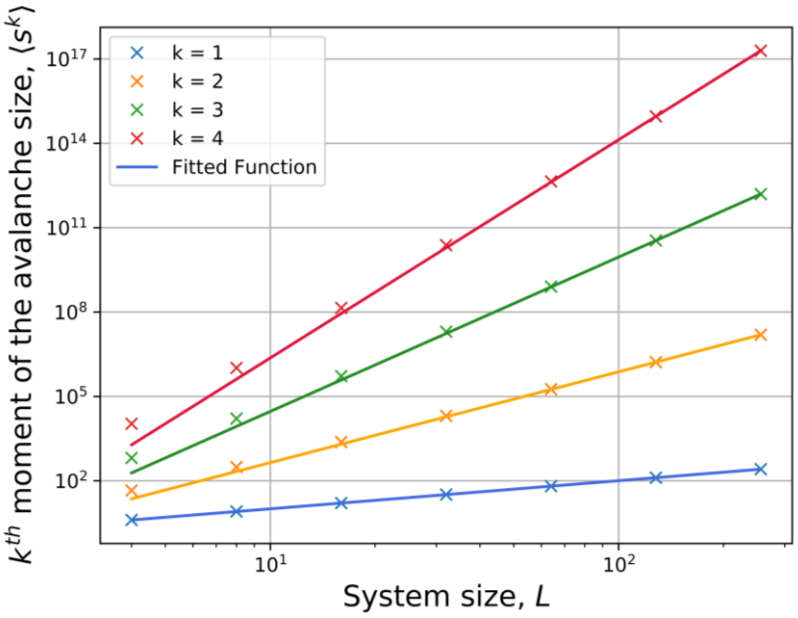

Fig. 15. The measured k^{th} moments as a function of system size. The fitted functions are power laws neglecting corrections to scaling, hence are only valid for $L \gg 1$. The data therefore deviates from the fit for smaller system sizes. The exponent of the power law is $D(1 + k - \tau_s)$ and is estimated using a minimisation of least squares fit.

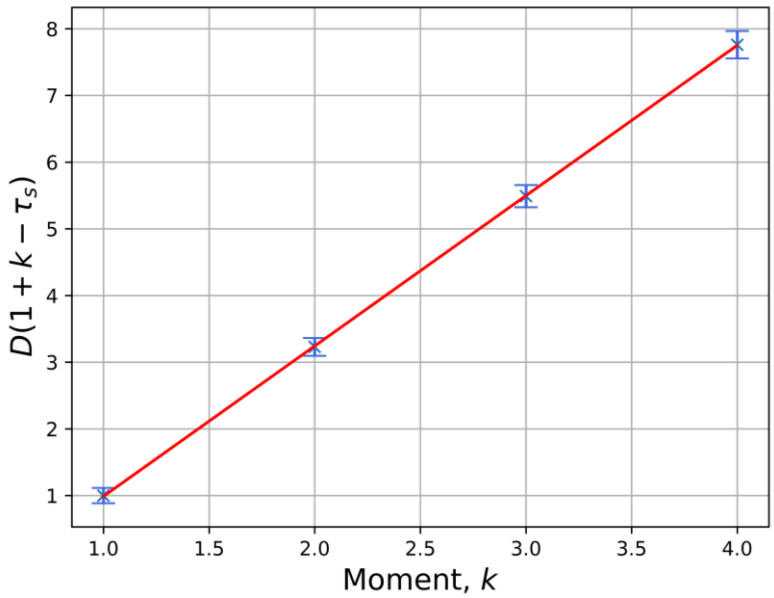

Fig. 16. The power law exponents in equation (35) measured from Fig. 15 as a function of the moment. The relationship is clearly a straight line with gradient D intercepting the k-axis at $\tau_s - 1$. The critical exponents D and τ_s are thus determined from this plot to be 2.25 ± 0.05 and 1.56 ± 0.05 respectively. Error bars on the exponent increase with moment k since higher order moments are subject to large avalanches dominating the moment.

D. Corrections to scaling for critical exponents

Corrections to scaling in Fig. 15 are revealed by plotting $\langle s^k \rangle / L^{D(1+k-\tau_s)}$ against system size L, as in Fig. 17. This removes the L dependencies of $\langle s^k \rangle$, and therefore gives a straight horizontal line with a y-intercept of 1 in the absence of corrections to scaling. For $k > 1$, substantial corrections to scaling are required for small systems, but diminish as system size increases, approaching constants. This suggests minimal corrections to scaling are required for very large systems and none are required for infinite systems. The first moment exhibits minimal corrections to scaling for all system sizes, thus $\langle s \rangle = L$ is true of all systems in the steady state.

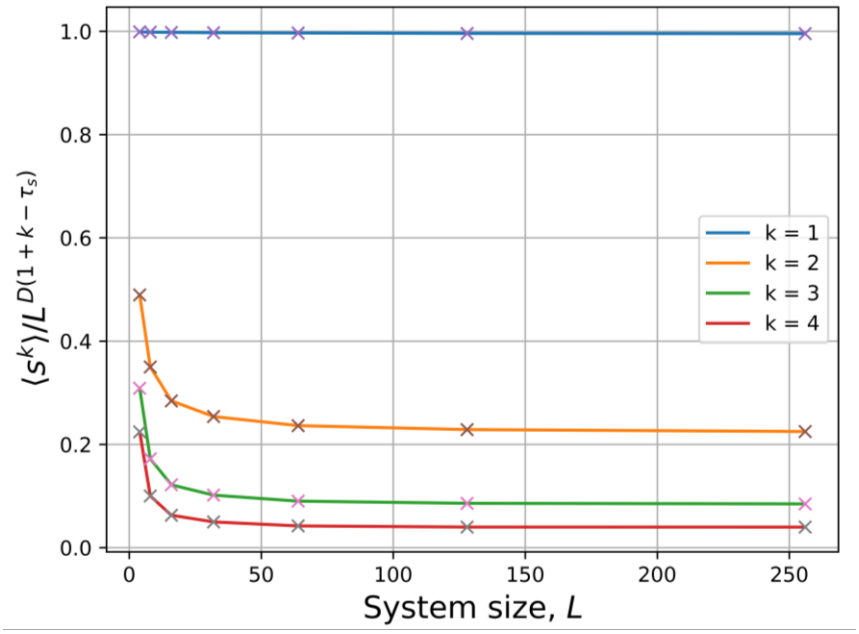

Fig. 17. The corrections to scaling for the measured k^{th} moments. For $k > 1$, there are significant corrections to scaling for small system sizes, whereas the $k = 1$ moment agrees exactly with theoretical models and no corrections to scaling are required. The plots for all moments tend towards constants for large system sizes, indicating that larger system sizes do not require significant corrections to scaling.

V. CONCLUSION

The Oslo model is implemented for a range of system sizes $L = \{4, 8, 16, 32, 64, 128, 256\}$ using a Python simulation. The height probabilities and avalanche size probabilities are subsequently investigated and the mathematical form of corrections to scaling is deduced. A finite-size scaling ansatz is proposed to model corrections to scaling and the critical exponents D and τ_s are estimated using the data collapse and moment analysis. Using the data collapse $D = 2.25 \pm 0.05$ and $\tau_s = 1.54 \pm 0.05$, and using moment analysis $D = 2.25 \pm 0.05$ and $\tau_s = 1.56 \pm 0.05$. For large system sizes $L \gg 1$, corrections to scaling for the k^{th} moments tend to zero. Corrections to scaling for the 1st moment are not significant for any system size.

VI. REFERENCES

[1] Bak P, Tang C, Wiesenfeld K. Self-organized criticality. Physical review A. 1988 Jul 1;38(1):364.
[2] Frette V, Christensen K, Malthe-Sørenssen A, Feder J, Jøssang T, Meakin P. Avalanche dynamics in a pile of rice. Nature. 1996 Jan;379(6560):49-52.

[3] Christensen K, Moloney NR. Complexity and criticality. World Scientific Publishing Company; 2005 Oct 3.
[4] Christensen K, Complexity Project Notes, 2020, Imperial College London

VII. ACKKNOWLEDGEMENTS

I would like to thank Max Falkenberg McGillivray for their log-binning code applied to the data in Fig. 11.